NANO LETTERS

pubs.acs.org/NanoLett Letter

Distinguishing Thermal from Nonthermal ("Hot") Carriers in Illuminated Molecular Junctions

Yonatan Dubi,* Ieng-Wai Un, and Yonatan Sivan

Cite This: *Nano Lett.* 2022, 22, 2127−2133 Read Online

ACCESS | Metrics & More | Article Recommendations | Supporting Information

ABSTRACT: The search for the signature of nonthermal (so-called "hot") electrons in illuminated plasmonic nanostructures requires detailed understanding of the nonequilibrium electron distribution under illumination, as well as a careful design of the experimental system employed to distinguish nonthermal electrons from thermal ones. Here, we provide a theory for using plasmonic molecular junctions to achieve this goal. We show how nonthermal electrons can be measured directly and separately from the unavoidable thermal response and discuss the relevance of our theory to recent experiments.

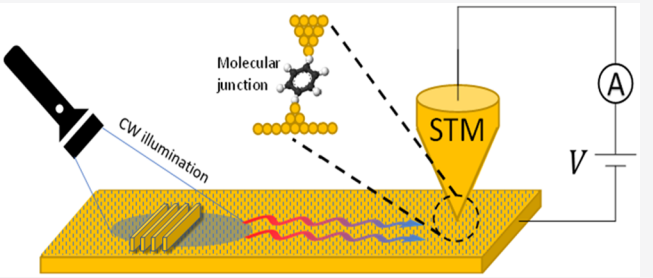

KEYWORDS: *plasmonics, electron nonequilibrium, molecular junctions, hot carriers*

Downloaded via BEN GURION UNIV OF THE NEGEV on April 13, 2022 at 09:32:54 (UTC).
See https://pubs.acs.org/sharingguidelines for options on how to legitimately share published articles.

INTRODUCTION

When a plasmonic nanostructure is continuously illuminated, two things happen simultaneously. First, the system unavoidably heats up, and second, nonthermal (so-called "hot") carriers (NTCs) are generated. The latter effect leads to an electron (and hole) distribution that deviates from the equilibrium (Fermi−Dirac) distribution.[1,2] There has been growing interest in understanding the interplay between these two processes; nonthermal carriers were suggested to be beneficial for various applications, including, notably, photodetection,[3−7] and plasmon-driven chemistry.[8−14] However, the latter application is very sensitive to the temperature of the system. Thus, distinguishing between NTCs and thermal effects is crucial for understanding how (and if at all) NTCs can be used to catalyze certain reactions.

Various indirect ways were proposed to determine the nonthermal electron population. These primarily include the study of the ultrafast dynamics of the metal permittivity via transient reflectivity measurements[15−19] and of the photoemission[20−23] following illumination by an ultrashort pulse. Under such conditions, a relatively large number of high-energy nonthermal electrons are being generated, but it is not clear when and how to separate those from mere heating. In contrast, under continuous wave illumination, it is clear that the information about heating is characterized by Fermi-like distribution of carriers close to the Fermi level, whereas the NTCs reside further away from the Fermi level in nearly flat "shoulders" (see refs 2 and 24). However, the practical separation between thermal and nonthermal carriers is very challenging, because the number of the high-excess-energy nonthermal electrons is many orders of magnitude smaller than the number of thermal (i.e., low excess energy) carriers. Thus, the various attempts made to directly quantify the contributions of these two types of charge carriers (e.g., to chemical reaction rates in the context of plasmon-assisted photocatalysis) frequently fail,[25−28] because the control thermocatalysis (light off) experiments must reproduce exactly the temperature profile of the photocatalysis (light on) experiments,[14,26] a task which is nearly impossible (although progress has been made in this direction).[29−34]

In an attempt to circumvent this problem, Reddy, Wang, and coauthors[35] recently suggested measuring directly the NTC distribution by coupling a plasmonic Au film to a molecular junction (schematically described in Figure 1(a), adapted from ref 35). By measuring the $I-V$ curves through the molecular junction (MJ) under illumination and in the dark, these authors assess directly the effect of illumination on the electronic distribution in the illuminated Au electrode.

The theoretical foundations to describe the nonthermal electron distribution as well as the current through such a plasmonic MJ were laid in ref 1. We recently extended the first part of the model of ref 1 to provide a complete model of the electron nonequilibrium under CW illumination.[2,24] Here, we extend the second part of the theory of ref 1, namely, transport through a MJ coupled to two electrodes, by combining the standard Landauer theory of transport through MJs[36,37] and the analytic form for the electron nonequilibrium distribution

Received: November 7, 2021
Revised: January 16, 2022
Published: January 25, 2022

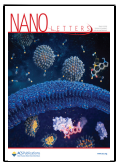

© 2022 American Chemical Society

https://doi.org/10.1021/acs.nanolett.1c04291
Nano Lett. 2022, 22, 2127−2133

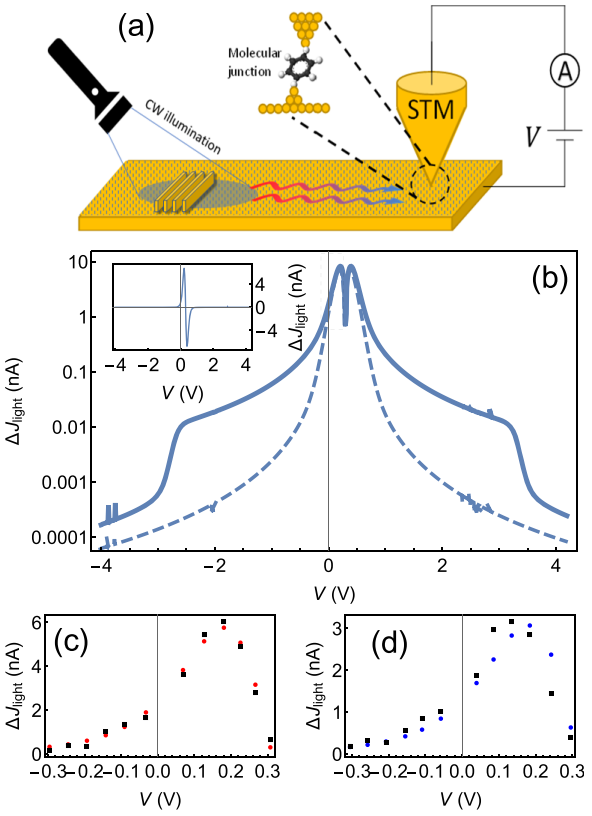

Figure 1. (a) Schematic depiction of the experimental setup, comprising an Au slab with nanofabricated gratings, and a molecular junction (MJ) formed between the slab and an STM tip. Surface plasmons are excited in the slab by CW illumination of the grating, and propagate toward the MJ (wiggly arrows). (b) ΔJ_{light} (3) as a function of bias voltage (log scale) for a molecular junction with resonance close to the Fermi level, with parameters $\mathcal{E}_0$= 0.15 eV and Γ = 10 meV, and setting $T_{\text{e,bottom}}$ = 305 K, $T_{\text{e,top}} = T_{\text{dark}}$ = 300 K and $\delta_{\text{E}}(1) = 10^{-5}$ (see text for further details). Near zero bias, the most dominant feature is the thermal contribution to the current. Spikes in the plot correspond to voltages at which the current changes sign. The dashed line shows ΔJ_{light} without illumination, i.e., all parameters are the same except $\delta_{\text{E}}(1) = 0$, thus showing only the thermal response. The dashed black square shows the region of measurement in ref 35 (note the match between solid and dashed lines in this region, marking that nonthermal effects are negligible there). Inset: same plot in linear scale. (c–d) Fits to experimental data of Reddy et al.,[35] for (c) 6 nm and (d) 13 nm thick slabs, assuming that the tip is not heated but the slab right under it is. Molecular parameters were set to $\mathcal{E}_0$ = 0.155 eV and Γ = 0.057 eV. Red and blue circles are the experimental data, and black squares are the fits, yielding δT = 2.21 and 1.14 K for (c) and (d) respectively (see text for further discussion on these parameters).

of an illuminated metal,[24] and we suggest a scheme that can be used to measure the nonthermal electron distribution in the presence of strong heating and even large thermal gradients (i.e., regardless of the temperature distribution). Using this formulation we shed new light on the experimental results of Reddy and Wang et al.,[35] demonstrating that it is possible that they indeed were able to distinguish (probably for the first time) nonthermal electrons from thermal ones, but not in the way interpreted in the original manuscript. Specifically, we show that the signature of nonthermal electrons is weak in some of the key measurements of ref 35, which can be explained alternatively via a purely thermal model. However, we point out that the signature of nonthermal electrons is dominant in some other experiments that have been performed by the authors of ref 35.

RESULTS AND DISCUSSION

General Theory. Current through a molecular junction is typically described by the Landauer formula,[36,37] which relates the total current to the electronic transmission function $\mathcal{T}(\mathcal{E})$ and the electrodes' electron distribution functions, $J = \frac{2e}{\hbar}\int \mathrm{d}\mathcal{E}\,\mathcal{T}(\mathcal{E})(f_{\text{top}} - f_{\text{bottom}})$ where, e is the electron charge, h is Planck's constant, and $f_{\text{top/bottom}}$ represent the electron distribution of the top/bottom electrodes (representing the STM tip and the Au slab, respectively); see Figure 1a. At equilibrium, $f_{\text{top}} = f_{\text{bottom}} = f^T(\mathcal{E}, T_{\text{e}})$, where $f^T(\mathcal{E}, T_{\text{e}}) = \left(1 + \exp\left(\frac{\mathcal{E}-\mu}{k_{\text{B}}T_{\text{e}}}\right)\right)^{-1}$ is the thermal (Fermi–Dirac) distribution, T_{e} is the (electron) temperature, μ is the chemical potential, and k_{B} is the Boltzmann constant. The transmission function is typically described by a Lorentzian, $\mathcal{T}(\mathcal{E}) = \frac{\Gamma^2}{\Gamma^2 + (\mathcal{E}-\mathcal{E}_0)^2}$, where $\mathcal{E}_0$ is the energy of the frontier molecular orbital and Γ is the level broadening (this is the so-called wideband approximation).[36,37] Notably, the Landauer formula implicitly assumes that the electron and temperature distributions on the electrodes are uniform. We point that this approach ignores the direct effect of illumination on the electrons in the molecule, which is justified because the illumination is off-resonance with the molecular HOMO–LUMO gap (and also with $\mathcal{E}_0 - \mu$ which may affect transport);[38] hence, the effect is negligible. It also disregards electron interactions in the molecule, which may shift the resonance position, but steal lead to Lorentzian-like transmission.[39,40] These approximations were also used in ref 35.

With equal distributions on the two electrodes, the current vanishes. As bias voltage V is applied, the chemical potentials shift such that $\mu_{\text{top}} - \mu_{\text{bottom}} = eV$ and current flows through the junction (we hereafter treat voltage in units of electronvolt, eV). Current can also be driven by a temperature difference (i.e., setting $T_{\text{e,top}} \neq T_{\text{e,bottom}}$), generating a thermo-electric effect.[36,37,41]

For the current to give an indication on the nonthermal electron distribution, it needs to be generated using optical illumination in an asymmetric manner, such that electric field felt by the electrodes is substantially different, and as a result, $f_{\text{top}} \neq f_{\text{bottom}}$.[42−45] The MJ geometry enables this naturally; indeed, electromagnetic and thermal simulations of a generic MJ geometry reveal significant differences in the local fields and temperature across the MJ (see the Supporting Information, section 3.1). To evaluate this effect, we follow ref 24 (specifically its Appendix A), where it was shown that under continuous illumination (i.e., by monochromatic light at frequency ω_{L}), the electron distribution in a Drude metal is (to an excellent approximation)

$$f(\mathcal{E};\, T_{\text{e}},\, \omega_{\text{L}},\, |E|^2) = f^T(\mathcal{E};\, T_{\text{e}}) + \delta_{\text{E}}(\mathcal{E};\, T_{\text{e}})\left((1 - f^T(\mathcal{E};\, T_{\text{e}}))f^T(\mathcal{E} + \hbar\omega_{\text{L}}) + f^T(\mathcal{E};\, T_{\text{e}})(1 - f^T(\mathcal{E} - \hbar\omega_{\text{L}}))\right) \quad (1)$$

where δ_{E} measures the population of nonthermal carriers, or more precisely the deviation of the distribution function from its equilibrium form, and is given by

https://doi.org/10.1021/acs.nanolett.1c04291
Nano Lett. 2022, 22, 2127−2133

$$\delta_E(\mathcal{E}, T_e) \equiv \left|\frac{E}{E_{sat}}\right|^2, \quad |E_{sat}(\mathcal{E}, T_e)|^2 \equiv \frac{1}{\tau_{e-e}(\mathcal{E}, T_e)R} \tag{2}$$

Here, $|E|^2$ is the local electric field intensity and R is a constant that depends on the (imaginary part of the) metal permittivity at the laser frequency ϵ''_m, and electron density n_e but not on T_e (see the Supporting Information, section 3.1). The expression for R in the original derivation[24] had a small typo; it was corrected in an errata and is noted in ref 46. The e−e collision rate is $\tau_{e-e}(\mathcal{E}, T_e) = \{K[(\pi k_B T_e)^2 + (\mathcal{E}-\mu)^2]\}^{-1}$, for which we adopt the Fermi liquid theory, with K being the e−e scattering constant.[47] The importance of high-energy nonthermal (i.e., "hot") carriers, via the change in the distribution due to hot carriers, can be simply quantified by evaluating $\delta_E(1) = \delta_E(\mathcal{E} - \mu = 1\ \text{eV})$, namely, the value of δ_E at an energy 1 eV above the Fermi energy, which captures the deviation from a thermal distribution at high energies. Notably, the solution for the nonequilibrium distribution (eq 1) is also obtained under the assumption of uniform (or averaged) field. We point out that while other formulations of the electron nonequilibrium exist, their limitations (see the discussion in refs 2 and 24) make them unsuitable for separating thermal from non-thermal effects.

Evaluating the current through an asymmetrically illuminated MJ can now be easily done by setting $f_{top} = f(\mathcal{E} + V; T_{e,top}, |E_{top}|^2)$and $f_{bottom} = f(\mathcal{E}; T_{e,bottom}, |E_{bottom}|^2)$ (assuming that the bottom electrode is grounded)[35] and plugging these distributions into the Landauer formula for the current. To isolate the contribution of illumination, we follow the authors of ref 35 who subtracted from the current under illumination the current in the dark (both as a function of voltage). In this case, the contribution to the current from illumination is simply

$$\Delta J_{light} = J_{light}(V, T_{e,top}, T_{e,bottom}, |E_{top}|^2, |E_{bottom}|^2) - J_{dark}(V, T_{dark}) \tag{3}$$

Equation 3 implies that the current is determined by the electric field and electron temperature rise induced by the illumination at both electrodes. We use numerical simulations to evaluate these quantities, and then we evaluate ΔJ_{light} for various molecular and illumination conditions. We show below that depending on the properties of the molecular system ΔJ_{light} has a dominant feature coming from either the temperature difference or the NTC contribution.

Results: Nearly Resonant Molecules. We start with addressing a "nearly resonant" molecule (i.e., a molecule for which the orbital energy is close to the electrodes' Fermi level); generally, it can represent either the HOMO or LUMO levels in the molecule, depending on the molecular moiety. In Figure 1b, we plot (the log of the absolute value of) ΔJ_{light} as a function of voltage for a molecular junction, taking relevant parameters for a typical MJ, $\mathcal{E}_0 = 0.15$ eV and $\Gamma = 10$ meV; the relatively small value of $\mathcal{E}_0$ makes this molecule "nearly resonant" (with respect to the electrodes' Fermi level). We take $\delta_E(1) = 1.5 \times 10^{-5}$ (which corresponds to the value we calculate from microscopic consideration, see the Supporting Information, section 3) and $\hbar\omega_L = 1.48$ eV (corresponding to 833 nm wavelength); note that the chosen wavelength is sufficiently longer than the ∼1.77 eV threshold for interband transitions,[48] thus validating the use of the analytic solution for Drude metals (eqs 1 and 2). We further set $T_{dark} = 300$ K and assume that the illuminated slab under the STM tip is heated by 5 K (i.e., $T_{e,bottom} = 305$ K). These parameters are close to those presented in ref 35. We also assume (as in ref 35) that the STM tip itself is not heated ($T_{e,top} = T_{dark}$).

In this case, since the nonthermal part of the distribution is negligible for realistic values of voltage bias (ca. ±0.3 V in ref 35), the contribution of the light to the current is given by[35]

$$\begin{aligned}\Delta J_{light} &= \frac{2e}{h}\int d\mathcal{E}\, \mathcal{T}(\mathcal{E} + V/2)\{f^T(\mathcal{E}; T_{e,bottom}) - f^T(\mathcal{E} + V; T_{e,top}) - (f^T(\mathcal{E}; T_{dark}) - f^T(\mathcal{E} + V; T_{dark}))\} \\ &\simeq \frac{2e}{h}\int d\mathcal{E}\, \mathcal{T}(\mathcal{E} + V/2)\{f^T(\mathcal{E}; T_{e,bottom}) - f^T(\mathcal{E}; T_{dark})\}\end{aligned} \tag{4}$$

ΔJ_{light} is plotted in Figure 1b, showing two prominent features. The first is that the strongest current occurs at low voltages, close to $\mathcal{E}_0$; this is due to a thermal effect (coming from the heating of the slab under illumination), centered a width ∼Γ around the orbital resonance $\mathcal{E}_0$.[36,41] Specifically, the absolute value of T_{dark} has only a minor effect on the results of Figure 1b; it is the difference between the temperature of the bottom electrode upon illumination and its temperature in the dark which is responsible for the large changes near $V = 0$. In that regard, this thermal feature is not a "thermo-electric" effect, meaning that increasing the tip temperature (and hence, modifying the temperature difference between the electrodes) has a negligible effect on the current difference ΔJ_{light}. The second feature is the onset of nonthermal electron "shoulders"[2] in ΔJ_{light}, which extend into the high-voltage regime, where the thermal effect becomes small. Figure 1b shows "spikes" or dips in ΔJ_{light}. These are simply changes of sign in ΔJ_{light} which appear as spikes in the log plot, and do not have any special physical meaning (see the inset to Figure 1b, which shows the same data on a linear scale).

Armed with these insights from Figure 1b (mainly that at low bias voltages thermal effects are dominant for a nearly resonant molecule), we used eq 3 to fit the measured values of ΔJ_{light} of ref 35 for their L1 molecule (a charge-transfer complex of quaterthiophene (T4) and tetracyanoethylene (TCNE) with terminal thiophenes containing gold-binding methyl sulfides; data extracted from the Supporting Information Figure S16A in ref 35). We use data from two sets of measurements in ref 35, using Au slabs with thicknesses 6 and 13 nm. We set as free parameters both the molecular parameters $\mathcal{E}_0$ and Γ and the local temperature in the Au slab segment directly under the STM tip, $T_{e,bottom} = T_{dark} + \delta T$, where T_{dark} is the ambient temperature and δT is the excess temperature of the slab above ambient; we again assume that the top electrode remains unheated. We simultaneously fit both data sets with the same $\mathcal{E}_0$ and Γ, leaving only δT to vary between experiments.

In Figure 1c,d, we plot the experimental data and a best fit to eq 3 (black squares) with the common parameters $\mathcal{E}_0$ 0.155 eV and Γ = 0.057 eV, with $\delta T = 2.21$ and 1.14 K for the 6 and 13 nm slabs (red and blue circles, respectively). These fits indicate that a thermal origin for the experimental results is plausible. Importantly, associating ΔJ_{light} with a thermal effect naturally

https://doi.org/10.1021/acs.nanolett.1c04291
Nano Lett. 2022, 22, 2127−2133

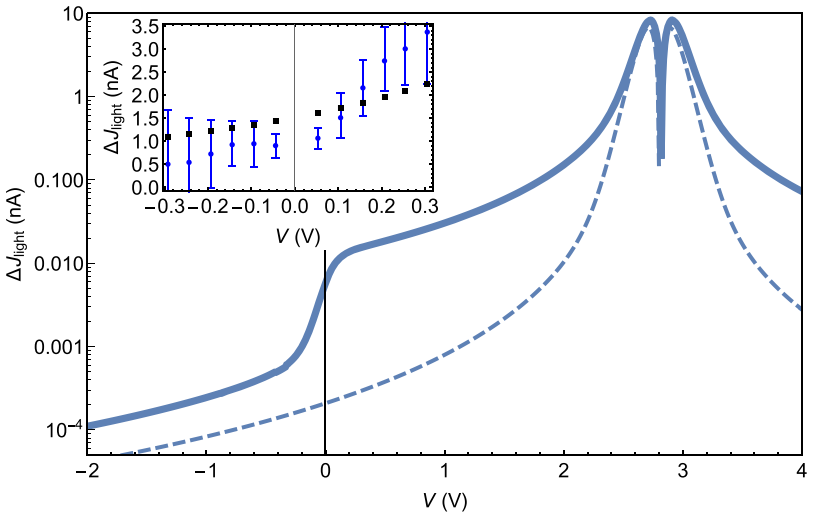

Figure 2. ΔJ_{light} (see eq 3) as a function of bias voltage (log scale) for a molecular junction with molecular resonance $\mathcal{E}_0$ = 1.4 eV far to the Fermi level, but in resonance with the illumination frequency. We take $\delta_{E,top}(1) = 1 \times 10^{-5}$ and $\delta_{E,bottom}(1) = 0$, and all other parameters are the same as for L1 (see text for details). Dashed line: same parameters, without any NTCs, showing that the thermal contribution in these case is negligible near the Fermi level. Inset: fit between experimental data for molecule L2 and a 6 nm slab (Figure S18 of ref 35, blue circles) and theory (black squares), demonstrating that this measurement may indeed be an indication for NTCs. The molecular parameters Γ = 0.18 eV and $\mathcal{E}_0$ = 0.77 eV and $\delta_{E,top}(1) = 8 \times 10^{-6}$ (and keeping $\delta_{E,bottom}(1) \approx 0.1\delta_{E,top}(1)$) (see text for details).

explains the two energy scales appearing in the data (the position of the peak $\mathcal{E}_0$ and the line width Γ), which, in contrast, cannot be associated with any feature of NTCs (e.g., in eq 2). Note that while these same results were interpreted in ref 35 as the "hot" carrier contribution, no direct fit between theory and experiment was presented in ref 35. In fact, while it is customary to refer to "hot" electrons in the energy range close to the Fermi energy, the match of our Drude-based analysis to the measured data confirms that in this energy range there is predominantly only thermal electrons (i.e., electrons that are characterized by a Fermi−Dirac distribution (with a temperature potentially higher than ambient)), whereas the number of true nonthermal electrons is much smaller (proportional to $\delta_E(\mathcal{E} \sim \mathcal{E}_0 \pm \Gamma) \ll 1$). An exception to this statement may occur in the presence of interband transitions, due to the minute deviation of the distribution from equilibrium discussed in Figure 2a of ref 2.

Finally, we note that our best fit parameters mentioned above yield a rather small temperature rise in the Au slab below the STM tip (∼1−2 K). In the Supporting Information (section 3.2), we explain why these values, as well as the negligible heating assumed in both ref 35 and our analysis, are likely to match numerical thermal simulations of the experimental system for the (hard-to-simulate) several micrometer-wide STM tip, as indeed these were supposedly used in ref 35. Moreover, we show in the Supporting Information (section 2) that the data of ref 35 can be fit even to different slab temperatures.

Despite the compelling match of the fit and our simulations and analysis, a few words of caution are in order. Our fits seem to be somewhat inconsistent with some of the data presented in ref 35. For instance, the fitted values for $\mathcal{E}_0$ and Γ are different from those obtained in ref 35 (although the estimates in ref 35 are also inconsistent with some of their data; see Supporting Information section 1), but are consistent with earlier measurements of a similar junction.[49] Our results also show a discrepancy with the control experiments performed in ref 35, where current in the dark was measured at increased temperatures (ref 35 Figure S12), and showed essentially no sign of being temperature sensitive. However, these control experiments are inconsistent with the formalism and parameters used within ref 35. Indeed, plugging the ref 35 parameters into a calculation of the current reveals a strong dependence on temperature (for the same parameters of ref 35, Figure S12), yet no such temperature dependence was measured (see Supporting Information section 3.3 for further discussion).

Off-Resonance Molecule. The difficulty in distinguishing between the thermo-electric and nonthermal electron contributions to ΔJ_{light} stems from the two following points: (i) One cannot directly measure the sample temperature under the STM tip, and (ii) because of the relatively small $\mathcal{E}_0$ (the nearly resonant nature of the molecule) and the fact that thermal current response is limited to a width ∼Γ around the molecular orbital energy $\mathcal{E}_0$,[36,41] the thermal effect is most important for low (hence realistic) voltages (i.e., for molecular resonances around the Fermi level).

Overcoming the first point is very challenging. However, overcoming the second point is actually quite easy. In a molecular junction where the molecular orbital energy $\mathcal{E}_0$ is far from the Fermi level but in resonance with the illumination energy (i.e., $\mathcal{E}_0 \sim \hbar\omega_L$), low-voltage measurements of ΔJ_{light} will only show the nonthermal part of the distribution. This is because, as is evident from eq 1 and the Landauer formula, the nonthermal features extend to a distance $\hbar\omega_L$ from the molecular resonance, and will thus be prominent at low voltages.

In this case, since the thermal contribution is negligible, the contribution of the illumination to the current is given by

$$\Delta J_{light} \approx \frac{2e}{h}\int d\mathcal{E}\, \mathcal{T}(\mathcal{E} + V/2)\{\delta_{E,bottom} f^T(\mathcal{E} - \hbar\omega_L, T_{e,bottom}) - \delta_{E,top} f^T(\mathcal{E} + V - \hbar\omega_L; T_{e,top})\} \quad (5)$$

https://doi.org/10.1021/acs.nanolett.1c04291
Nano Lett. 2022, 22, 2127−2133

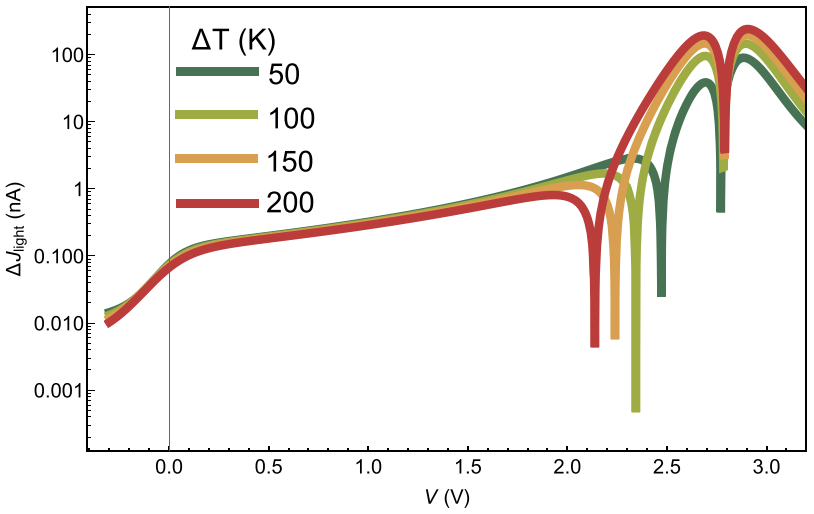

Figure 3. ΔJ_{light} (3) as a function of bias voltage (log scale) for different values of electron temperature, $T_{\text{e,bottom}} = T_{\text{dark}} + 50$, 100, 150, and 200 K (see text for other parameters). The thermal effect (which appears close to the molecular resonance) strongly depends on temperature, while the NTCs contribution is temperature independent, thus providing a simple way for discriminating between the two effects.

where $\delta_{\text{E,bottom/top}}$ are derived (using eq 2) from the local field on the bottom/top electrodes. Note that in eq 5 only electrons are considered (i.e., the correction to the distribution corresponding to holes ($\sim f(\mathcal{E} + \hbar\omega_{\text{L}})$) is disregarded), since holes will shift the distributions further away from the resonance and will not contribute to ΔJ_{light}.

In Figure 2, we plot (the log of) ΔJ_{light} as a function of bias voltage (as in Figure 1b) for the case of $\mathcal{E}_0 = 1.4$ eV, at resonance with $\hbar\omega_{\text{L}}$ (all other parameters are the same as for L1, solid line), for $\delta_{\text{E,top}}(1) = 1 \times 10^{-5}$ and $\delta_{\text{E,bottom}}(1) = 0$. It is clear that now the thermal feature only appears at high (hence, inaccessible) voltages, while at low voltages, the nonthermal electron "shoulder" provides the prominent contribution to the current. For comparison, the dashed line shows ΔJ_{light} for $\delta_{\text{E,bottom}}(1) = 0$ (i.e., no nonthermal electrons), demonstrating the orders-of-magnitude larger contribution of nonthermal electrons at low voltages. Importantly, there are also qualitative differences with respect to a nearly resonant molecule like L1; the most prominent is the fact that ΔJ_{light} does not change sign, a feature which can be easily recognized experimentally (indeed, see below).

A somewhat similar experiment was, in fact, conducted in ref 35, using a MJ with a 1,4-benzenediisonitrile molecule (dubbed L2 in ref 35). This molecule has a LUMO level which is far from the Fermi level, $\mathcal{E}_{\text{LUMO}} - \mu \sim 0.77$ eV,[50] and thus is somewhat similar to the situation described above. In the Supporting Information of ref 35 (Figure S18), the authors plot ΔJ_{light} vs the bias voltage. We use these data to fit eq 3, and we find that for this molecular energy indeed the thermal contribution is negligible for that range of voltages and that the data can be fit very well (within the experimental error) with the contribution coming solely from the nonthermal part of the distribution. This is shown in the inset to Figure 2 where the experimental data (blue points) and the theoretical points (black squares) are shown. The molecular parameters $\Gamma = 0.18$ eV and $\mathcal{E}_0 = 0.77$ eV are taken from ref 50, and the only fit parameters are $\delta_{\text{E,bottom}}(1)$ and $\delta_{\text{E,top}}(1)$.

To reduce further the number of fit parameters, we have conducted numerical simulations of the electric field under the experimental conditions (see Supporting Information section 3.1). These simulations show that the field in the tip is actually larger than the field in the slab by a factor of ~3.2, due to the plasmonic enhancement around the tip.

In the inset to Figure 2, we plot the experimental data of ref 35 (blue points, along with the experimental error bars) and the theoretical ΔJ_{light} as a function of bias voltage, where $\delta_{\text{E,top}}(1) = 8 \times 10^{-6}$ (keeping $\delta_{\text{E,bottom}}(1) \approx 0.1\delta_{\text{E,top}}(1)$) is found to provide the best fit value. This fit between data and theory provides further experimental corroboration to eq 3, providing what is, to the best of our knowledge, the first direct measurement of the steady-state nonthermal contribution to the electron distribution. These values for δ_{E} match the calculated values for the electric field (see Supporting Information section 3.1) and are in good correlation with reported "hot" electron efficiencies in plasmon-assisted photocatalysis experiments.[29,32,51]

However, somewhat unintuitively, the experimental data of the L2 molecule in ref 35 can also be explained by simple heating. Indeed, by setting the δ_{E} values to zero and assuming $\delta T_{\text{e,bottom}} \sim 20$ K, we obtain a fit essentially similar to that shown in the inset of Figure 2; this is not a contradiction with Figure 2, because the energy of molecule L2 obtained from the fit is much lower (i.e., not as far from resonance) compared with the value used for the illustration of Figure 2. In that respect, the experiment in ref 35 involves an intermediate case, whereby the molecular energy is only partially off-resonance. We thus face a situation where both NTCs and thermal effects can reproduce the experimental data.

Fortunately, unlike the situation in plasmon-assisted photocatalysis experiments (e.g., ref 25), the MJ setup offers a simple way to further discriminate between the two effects, by simply measuring ΔJ_{light} (for the off-resonance molecule) as a function of the ambient temperature. The reason is that while the thermal contribution would be strongly influenced by the temperature, the NTCs would not (see eq 1 and ref 24). In order to demonstrate this, in Figure 3, we plot ΔJ_{light} as a function of bias voltage for $T_{\text{e,bottom}} = T_{\text{dark}} + 50$, 100, 150, and 200 K, and as can be seen, the low-voltage NTC contribution to ΔJ_{light} is essentially unchanged. Another way to overcome the situation is to choose a molecular junction which has frontier orbitals which are even further away from the Fermi level of the electrodes, such as Au−benzenedithiol−Au

https://doi.org/10.1021/acs.nanolett.1c04291
Nano Lett. 2022, 22, 2127−2133

junctions, where the HOMO level is ∼1.2 eV away from the Fermi level.[52] Under such circumstances, the thermal effect is expected to contribute only a tiny fraction of the NTC contribution to ΔJ_{light}.

SUMMARY

In conclusion, we have shown that our analytical prediction of the electron distribution under continuous wave illumination can be used to interpret recent experiments (ref 35). This sheds new light on these experiments and demonstrates that they seem to directly measure the NTC contribution to the distribution function, however, surprisingly, not as they originally interpreted their data. We suggest further experiments that can be analyzed within our theory, and the necessary improvements to state-of-the-art theories for the electron nonequilibrium distribution and current through a MJ, thus providing a direct route to solving one of the outstanding questions in plasmonic systems, namely, the form of the electron distribution under continuous illumination. Finally, the methodology presented here can be used for as a starting point for a theoretical treatment of other experiments where nanoscale transport is coupled to plasmonic effects.[53,54,54−57]

ASSOCIATED CONTENT

Supporting Information

The Supporting Information is available free of charge at https://pubs.acs.org/doi/10.1021/acs.nanolett.1c04291.

Additional transport calculation details, fit parameters, and thermal calculations(PDF)

AUTHOR INFORMATION

Corresponding Author

Yonatan Dubi − *Department of Chemistry, Ben-Gurion University of the Negev, Be'er Sheva 8410501, Israel;* orcid.org/0000-0002-8988-4935; Email: jdubi@bgu.ac.il

Authors

Ieng-Wai Un − *School of Electrical and Computer Engineering, Ben-Gurion University of the Negev, Be'er Sheva 8410501, Israel;* orcid.org/0000-0002-7156-0019

Yonatan Sivan − *School of Electrical and Computer Engineering, Ben-Gurion University of the Negev, Be'er Sheva 8410501, Israel;* orcid.org/0000-0003-4361-4179

Complete contact information is available at: https://pubs.acs.org/10.1021/acs.nanolett.1c04291

Notes

The authors declare no competing financial interest.

REFERENCES

(1) Kornbluth, M.; Nitzan, A.; Seideman, T. Light-induced electronic non-equilibrium in plasmonic particles. *J. Chem. Phys.* **2013**, *138*, 174707.

(2) Dubi, Y.; Sivan, Y. Hot electrons" in Metallic Nanostructures - Non-Thermal Carriers or Heating? *Light: Sci. Appl.* **2019**, *8*, 89.

(3) Goykhman, I.; Desiatov, B.; Khurgin, J.; Shappir, J.; Levy, U. Locally Oxidized Silicon Surface-Plasmon Schottky Detector for Telecom Regime. *Nano Lett.* **2011**, *11*, 2219−2224.

(4) Goykhman, I.; Desiatov, B.; Khurgin, J.; Shappir, J.; Levy, U. Waveguide based compact silicon Schottky photodetector with enhanced responsivity in the telecom spectral band. *Opt. Exp.* **2012**, *20*, 28594.

(5) Mubeen, S.; Lee, J.; Singh, N.; Kraemer, S.; Stucky, G. D.; Moskovits, M. An autonomous photosynthetic device in which all charge carriers derive from surface plasmons. *Nat. Nanotechnol.* **2013**, *8*, 247−251.

(6) Li, W.; Valentine, J. Harvesting the Loss: Surface Plasmon-Based Hot Electron Photodetection. *Nanophotonics* **2017**, *6*, 177−191.

(7) Tagliabue, G.; Jermyn, A. S.; Sundararaman, R.; Welch, A. J.; DuChene, J. S.; Pala, R.; Davoyan, A. R.; Narang, P.; Atwater, H. A. Quantifying the Role of Surface Plasmon Excitation and Hot Carrier Transport in Plasmonic Devices. *Nat. Commun.* **2018**, *9*, 3394.

(8) Baffou, G.; Quidant, R. Nanoplasmonics for chemistry. *Chem. Soc. Rev.* **2014**, *43*, 3898.

(9) Robert, H. M. L.; Kundrat, F.; Bermúdez-Ureña, E.; Rigneault, H.; Monneret, S.; Quidant, R.; Polleux, J.; Baffou, G. Light-Assisted Solvothermal Chemistry Using Plasmonic Nanoparticles. *ACS Omega* **2016**, *1*, 2−8.

(10) Clavero, C. Plasmon-induced hot-electron generation at nanoparticle/metal-oxide interfaces for photovoltaic and photocatalytic devices. *Nat. Photonics* **2014**, *8*, 95−103.

(11) Wei, Q.; Wu, S.; Sun, Y. Quantum-Sized Metal Catalysts for Hot-Electron-Driven Chemical Transformation. *Adv. Mater.* **2018**, *30*, 1802082.

(12) Jain, P. K. Taking the Heat Off of Plasmonic Chemistry. *J. Phys. Chem.* **2019**, *123*, 24347−24351.

(13) Baffou, G.; Bordacchini, I.; Baldi, A.; Quidant, R. Simple Experimental Procedures to Discern Photothermal Processes in Plasmon-Driven Chemistry. *Light: Sci. Appl.* **2020**, *9*, 108.

(14) Sivan, Y.; Dubi, Y. Recent Developments in Plasmon-Assisted Photocatalysis - a Personal Perspective. *Appl. Phys. Lett.* **2020**, *117*, 130501.

(15) Groeneveld, R. H. M.; Sprik, R.; Lagendijk, A. Femtosecond spectroscopy of electron-electron and electron-phonon energy relaxation in Ag and Au. *Phys. Rev. B* **1995**, *51*, 11433−11445.

(16) Del Fatti, N.; Voisin, C.; Achermann, M.; Tzortzakis, S.; Christofilos, D.; Valleé, F. Nonequilibrium electron dynamics in noble metals. *Phys. Rev. B* **2000**, *61*, 16956−16966.

(17) Della Valle, G.; Conforti, M.; Longhi, S.; Cerullo, G.; Brida, D. Real-time optical mapping of the dynamics of nonthermal electrons in thin gold films. *Phys. Rev. B* **2012**, *86*, 155139.

(18) Masia, F.; Langbein, W.; Borri, P. Measurement of the dynamics of plasmons inside individual gold nanoparticles using a femtosecond phase-resolved microscope. *Phys. Rev. B* **2012**, *85*, 235−403.

(19) Stoll, T.; Maioli, P.; Crut, A.; Del Fatti, N.; Vallée, F. Advances in femto-nano-optics: ultrafast nonlinearity of metal nanoparticles. *Eur. Phys. J. B* **2014**, *87*, 260.

(20) Bauer, M.; Aeschlimann, M. Dynamics of excited electrons in metals thin films and nanostructures. *J. Electron. Spectroscop. Relat. Phenomen.* **2002**, *124*, 225−243.

(21) Bauer, M.; Marienfeld, A.; Aeschlimann, M. Hot electron lifetimes in metals probed by time-resolved two-photon photoemission. *Prog. Surf. Sci.* **2015**, *90*, 319−376.

(22) Vogelsang, J.; Robin, J.; Nagy, B. J.; Dombi, P.; Rosenkranz, D.; Schiek, M.; Gross, P.; Lienau, C. Ultrafast Electron Emission from a Sharp Metal Nanotaper Driven by Adiabatic Nanofocusing of Surface Plasmons. *Nano Lett.* **2015**, *15*, 4685−4691.

(23) Reutzel, M.; Li, A.; Gumhalter, B.; Petek, H. Nonlinear Plasmonic Photoelectron Response of Ag(111). *Phys. Rev. Lett.* **2019**, *123*, 017404.

(24) Sivan, Y.; Un, I. W.; Dubi, Y. Assistance of Plasmonic Nanostructures to Photocatalysis - Just a Regular Heat Source. *Faraday Discuss.* **2019**, *214*, 215−233.

(25) Sivan, Y.; Baraban, J.; Un, I. W.; Dubi, Y. Comment on "Quantifying Hot Carrier and Thermal Contributions in Plasmonic Photocatalysis. *Science* **2019**, *364*, No. eaaw9367.

(26) Sivan, Y.; Un, I. W.; Dubi, Y. Thermal Effects - an Alternative Mechanism for Plasmonic-Assisted Photo-catalysis. *Chem. Sci.* **2020**, *11*, 5017−5027.
(27) Dubi, Y.; Un, I. W.; Baraban, J.; Sivan, Y. Matters Arising in "Plasmon-driven carbon−fluorine ($C(sp^3)$−F) bond activation with mechanistic insights into hot-carrier-mediated pathways". *arXiv.org (Chemical Physics)*, May 13, 2021, 2105.06382, ver. 1. https://arxiv.org/pdf/2105.06382.
(28) Sivan, Y.; Baraban, J.; Dubi, Y. Experimental Practices Required to Isolate Thermal Effects in Plasmonic Photo-catalysis - Lessons from Recent Experiments. *OSA Continuum* **2020**, *3*, 483−497.
(29) Kamarudheen, R.; Castellanos, G. W.; Kamp, L. P. J.; Clercx, H. J. H.; Baldi, A. Quantifying Photothermal and Hot Charge Carrier Effects in Plasmon-Driven Nanoparticle Syntheses. *ACS Nano* **2018**, *12*, 8447−8455.
(30) Yu, S.; Jain, P. K. Plasmonic photosynthesis of C_1−C_3 hydrocarbons from carbon dioxide assisted by an ionic liquid. *Nat. Commun.* **2019**, *10*, 2022.
(31) Li, X.; Everitt, H. O.; Liu, J. Confirming nonthermal plasmonic effects enhance CO_2 methanation on Rh/TiO_2 catalysts. *Nano Res.* **2019**, *12*, 1906−1911.
(32) Welch, A. J.; DuChene, J. S.; Tagliabue, G.; Davoyan, A.; Cheng, W.-H.; Atwater, H. A. Nanoporous Gold as a Highly Selective and Active Carbon Dioxide Reduction Catalyst. *ACS Appl. Energy Mater.* **2019**, *2*, 164−170.
(33) Xu, X.; Dutta, A.; Khurgin, J.; Wei, A.; Shalaev, V. M.; Boltasseva, A. TiN@TiO2 Core−Shell Nanoparticles as Plasmon-Enhanced Photosensitizers: The Role of Hot Electron Injection. *Laser Photonics Rev.* **2020**, *14*, 1900376.
(34) Tiburski, C.; Boje, A.; Nilsson, S.; Say, Z.; Fritzsche, J.; Ström, H.; Hellman, A.; Langhammer, C. Light-Off in Plasmon-Mediated Photocatalysis. *ACS Nano* **2021**, *15*, 11535.
(35) Reddy, H.; Wang, K.; Kudyshev, Z.; Zhu, L.; Yan, S.; Vezzoli, A.; Higgins, S. J.; Gavini, V.; Boltasseva, A.; Reddy, P.; et al. Determining plasmonic hot-carrier energy distributions via single-molecule transport measurements. *Science* **2020**, *369*, 423−426.
(36) Cuevas, J. C.; Scheer, E. *Molecular Electronics: An Introduction to Theory and Experiment*; World Scientific: Singapore, 2010.
(37) Di Ventra, M. *Electrical Transport in Nanoscale Systems*; Cambridge University Press: Cambridge, UK, 2008.
(38) Zhou, J.; Wang, K.; Xu, B.; Dubi, Y. Photoconductance from exciton binding in molecular junctions. *J. Am. Chem. Soc.* **2018**, *140*, 70−73.
(39) Evers, F.; Korytár, R.; Tewari, S.; van Ruitenbeek, J. M. Advances and challenges in single-molecule electron transport. *Rev. Mod. Phys.* **2020**, *92*, 035001.
(40) Thoss, M.; Evers, F. Perspective: Theory of quantum transport in molecular junctions. *J. Chem. Phys.* **2018**, *148*, 030901.
(41) Dubi, Y.; Di Ventra, M. Colloquium: Heat flow and thermoelectricity in atomic and molecular junctions. *Rev. Mod. Phys.* **2011**, *83*, 131.
(42) Vadai, M.; Nachman, N.; Ben-Zion, M.; Burkle, M.; Pauly, F.; Cuevas, J. C.; Selzer, Y. Plasmon-induced conductance enhancement in single-molecule junctions. *J. Phys. Chem. Lett.* **2013**, *4*, 2811−2816.
(43) Arielly, R.; Ofarim, A.; Noy, G.; Selzer, Y. Accurate determination of plasmonic fields in molecular junctions by current rectification at optical frequencies. *Nano Lett.* **2011**, *11*, 2968−2972.
(44) Wang, T.; Nijhuis, C. A. Molecular electronic plasmonics. *Applied Materials Today* **2016**, *3*, 73−86.
(45) Banerjee, P.; Conklin, D.; Nanayakkara, S.; Park, T.-H.; Therien, M. J.; Bonnell, D. A. Plasmon-induced electrical conduction in molecular devices. *ACS Nano* **2010**, *4*, 1019−1025.
(46) Sivan, Y.; Dubi, Y. Theory of "Hot" Photoluminescence from Drude Metals. *ACS Nano* **2021**, *15*, 8724−8732.
(47) Coleman, P. *Introduction to Many Body Physics*; Cambridge University Press: Cambridge, UK, 2015.
(48) Guerrisi, M.; Rosei, R.; Winsemius, P. Splitting of the interband absorption edge in Au. *Phys. Rev. B* **1975**, *12*, 557−563.
(49) Wang, K.; Vezzoli, A.; Grace, I. M.; McLaughlin, M.; Nichols, R. J.; Xu, B.; Lambert, C. J.; Higgins, S. J. Charge transfer complexation boosts molecular conductance through Fermi level pinning. *Chemical science* **2019**, *10*, 2396−2403.
(50) Lee, W.; Kim, K.; Jeong, W.; Zotti, L. A.; Pauly, F.; Cuevas, J. C.; Reddy, P. Heat dissipation in atomic-scale junctions. *Nature* **2013**, *498*, 209−212.
(51) Kim, Y.; Smith, J. G.; Jain, P. K. Harvesting multiple electron−hole pairs generated through plasmonic excitation of Au nanoparticles. *Nat. Chemistry* **2018**, *10*, 763.
(52) Reddy, P.; Jang, S.-Y.; Segalman, R. A.; Majumdar, A. Thermoelectricity in molecular junctions. *Science* **2007**, *315*, 1568−1571.
(53) Evans, C. I.; Natelson, D. Remote excitation of hot electrons via propagating surface plasmons. *J. Phys. Chem. C* **2019**, *123*, 10057−10064.
(54) Agreda, A.; Sharma, D. K.; Viarbitskaya, S.; Hernandez, R.; Cluzel, B.; Demichel, O.; Weeber, J.-C.; Colas des Francs, G.; Kumar, G. V. P.; Bouhelier, A. Spatial Distribution of the Nonlinear Photoluminescence in Au Nanowires. *ACS Photonics* **2019**, *6*, 1240−1247.
(55) Cui, L.; Zhu, Y.; Abbasi, M.; Ahmadivand, A.; Gerislioglu, B.; Nordlander, P.; Natelson, D. Electrically Driven Hot-Carrier Generation and Above-Threshold Light Emission in Plasmonic Tunnel Junctions. *Nano Lett.* **2020**, *20*, 6067−6075.
(56) Cui, L.; Zhu, Y.; Nordlander, P.; Di Ventra, M.; Natelson, D. Thousand-fold Increase in Plasmonic Light Emission via Combined Electronic and Optical Excitations. *Nano Lett.* **2021**, *21*, 2658−2665.
(57) Agreda, A.; Viarbitskaya, S.; Smetanin, I. V.; Uskov, A. V.; Colas des Francs, G.; Bouhelier, A. Electrostatic Control over Optically Pumped Hot Electrons in Optical Gap Antennas. *ACS Photonics* **2020**, *7*, 2153−2162.

NOTE ADDED AFTER ASAP PUBLICATION

This paper was published ASAP on January 25, 2022. Additional updates were made to equation 1, Figures 1, and 2. The corrected version was reposted on February 2, 2022.

https://doi.org/10.1021/acs.nanolett.1c04291
Nano Lett. 2022, 22, 2127−2133